

Retraction

Retracted: Distributed Network Image Processing System and Transmission Control Algorithm

Security and Communication Networks

Received 26 December 2023; Accepted 26 December 2023; Published 29 December 2023

Copyright © 2023 Security and Communication Networks. This is an open access article distributed under the Creative Commons Attribution License, which permits unrestricted use, distribution, and reproduction in any medium, provided the original work is properly cited.

This article has been retracted by Hindawi, as publisher, following an investigation undertaken by the publisher [1]. This investigation has uncovered evidence of systematic manipulation of the publication and peer-review process. We cannot, therefore, vouch for the reliability or integrity of this article.

Please note that this notice is intended solely to alert readers that the peer-review process of this article has been compromised.

Wiley and Hindawi regret that the usual quality checks did not identify these issues before publication and have since put additional measures in place to safeguard research integrity.

We wish to credit our Research Integrity and Research Publishing teams and anonymous and named external researchers and research integrity experts for contributing to this investigation.

The corresponding author, as the representative of all authors, has been given the opportunity to register their agreement or disagreement to this retraction. We have kept a record of any response received.

References

- [1] P. Zaiyi, Y. Kun, and W. Chaobin, "Distributed Network Image Processing System and Transmission Control Algorithm," *Security and Communication Networks*, vol. 2021, Article ID 5517843, 10 pages, 2021.

Research Article

Distributed Network Image Processing System and Transmission Control Algorithm

Pu Zaiyi,¹ Yang Kun ,² and Wang Chaobin³

¹Network and Information Management Center, China West Normal University, Nanchong 670009, Sichuan, China

²Linyi Meteorological Bureau, Linyi, Shandong, China

³School of Computer Science, China West Normal University, Nanchong 637009, Sichuan, China

Correspondence should be addressed to Yang Kun; yangkun198311@163.com

Received 2 March 2021; Revised 9 April 2021; Accepted 28 April 2021; Published 7 May 2021

Academic Editor: Chi-Hua Chen

Copyright © 2021 Pu Zaiyi et al. This is an open access article distributed under the Creative Commons Attribution License, which permits unrestricted use, distribution, and reproduction in any medium, provided the original work is properly cited.

With the increasing use of Internet technologies, image data is spreading more and more on the Internet. Whether it is a social network or a search engine, a large amount of image data is generated. By studying the distributed network image processing system and transmission control algorithm, this paper proposes a more accurate gradient calculation method based on the SIFT algorithm. It is concluded that the performance of the proposed algorithm is slightly better than that of the original algorithm, so the system is implemented. On the basis of reducing the performance of the original algorithm, the dimension of the image features is effectively reduced. By comparing the influence of the image retrieval system in the single-machine environment and the distributed environment on the image feature extraction rate, it is proved that the system uses five distributed nodes to construct the image transmission system that achieves the best results in terms of machine cost and system performance. The random Gaussian orthogonal matrix is analyzed with good stability and performance. The OMP algorithm has good convergence and reconstruction performance. The MH-BCS-SPL reconstruction algorithm works best, and the PSNR decreases very smoothly in the process of increasing the packet loss rate from 0.1 to 0.6. The experimental results show that different orthogonal bases behave differently under different images. Overall, the BCS-SPL series algorithm has greatly improved the reconstruction effect compared with the traditional OMP algorithm.

1. Introduction

With the continuous development of various industries, especially the unprecedented development of Internet applications such as social media and search engines, the number and size of image data are rapidly expanding, and both image transmission and image processing face enormous challenges. The traditional image search algorithm first uses text to identify the image and then uses the text retrieval method to query similar images. However, this method takes a lot of time to process the image's early identification, and as the number of images increases, the text's method of identification is no longer applicable. Therefore, the appearance of image features based on the image content itself brings great convenience to image retrieval. With the development of economy and

communication technology, communication and communication between people have become more and more convenient. However, communication security has also become an issue of increasing concern. Previous communication equipment providers have less considered the security of information transmission. As users pay more and more attention to the security of information, it has also become a bargaining chip for major operators to compete, and communication security is put on the agenda. Overseas operators have very high requirements for communication network security. If they are found to be inconsistent with security requirements, equipment suppliers will suffer huge economic losses. Therefore, communication network security cannot be ignored. If the security is not solved well, it will directly affect social stability and national security.

The storage, processing, and transmission of massive image data have become the focus of many scholars at home and abroad. Kim [1] implemented a 4-channel image processing embedded system that allows users to view the status of the car anytime anywhere. In addition, a communication function that can transmit a 4-channel image on an embedded board is realized. Wright et al. [2] designed an image sensor that solves the real-world object recognition challenge by using a subspace method that uses an eigenspace object model created from the appearance of multiple reference objects. Mataei et al. [3] proposed an innovative device for simulating the saturation state of the road surface, taking photos from the drainage process of the road surface, and applying image processing methods to generate appropriate indicators for drainage quality assessment. Barceló et al. [4] proposed a new intelligent automatic method based on image processing and neural network for welding detection and analysis. The developed system can accurately detect welding defects and classify them into different categories. Borsos et al. [5] proposed a novel DNC setup in which the microscope image was captured and processed in real time by image analysis, the controlled variable being the (relative) number of particles, which was manipulated by temperature using feedback control methods. Xiao [6] researched the use of 3G/4G network and satellite communication by drones to transmit live video images to the headquarters' command center in real time, forming a set of real-time backhaul solutions for rapid deployment of rescue scenes. Wenchang and Tian [7] analyzed the influence of objective factors such as underwater environment, visibility on the quality of experimental video images, and the preliminary design of the video image data processing system in airborne live video recording and transmission system. Video image data processing research has laid a certain technical foundation. Computer image processing speed is fast, and digital signal is not easy to be distorted, so it has the characteristics of easy storage, easy transmission, and strong anti-interference ability [8]. Zhang et al. [9] designed an online insulator image acquisition and real-time processing system and integrated an online insulator image processing algorithm for hardware implementation, which greatly reduced the amount of data transmission, while avoiding manual participation. Zhang et al. [10] designed a rice grain counting and measuring system based on image processing and Bluetooth transmission technology to realize the extraction of the rice seed number. The two-dimensional code technology was used to identify rice seed samples, and the information statistics of each sample were realized. Cong et al. [11] designed a kind of infrared based on DSP6455, using Gigabit Ethernet and RapidIO hardware interface, in view of the complex system of the actual infrared image processing system and the long algorithm debugging period. He considered the processing performance and real-time performance of the system and built an image processing simulation platform. Li et al. [12] designed a high-speed serial RapidIO bus-based image processing system, which is transmitted to the DSP memory through the RapidIO bus for complex algorithm processing. On the basis of the intelligent tracking and obstacle-proof fire-fighting smart car,

Zhang et al. [13] joined the image processing function, enabling the car to independently find and identify the flame and realize the automatic fire extinguishing function. At the same time, the image captured by the camera is transmitted through the WiFi module to realize the function of remotely monitoring the car.

The main technique of the image processing system is to use the image as an input source, then retrieve a similar picture on the Internet, and output it as a result, presented to the user. Many search engine companies are now researching image transmission functions, but they still have not achieved satisfactory results. Finding a high-efficiency, high-accuracy image transmission method is critical to the development of image processing technology. Distributed networks, due to their fast processing speed, high accuracy, and convenient operation, have been widely studied by many research teams.

Many research teams have seized the opportunity to conduct comprehensive and in-depth research and analysis on distributed networks. Benchimol et al. [14] applied distributed networks in medicine, based on population-based health management data, to determine the incidence of IBD in Canada, prevalence, and trends in childhood IBD over time. Rupperecht et al. [15] applied a distributed network to network processing and described a distributed connection processing technique that uses delay partitioning to accommodate transient network skew in the cluster. Awad et al. [16] proposed an energy cost-distortion solution that integrates wireless network components and application layer features to provide sustainable, energy-efficient, and high-quality services for mobile medical systems. Zhou and Liang [17] used the blockchain credit enhancement system and intelligent contract technology to make light adjustments to the data structure of the distributed ledger for the actual needs of content distribution applications. Li [18] designed a new HAIPS active intrusion prevention model based on the distributed automation network, perfected the basic control flow of the bus, and realized the construction of the distributed automation network operation environment. Lan et al. [19] proposed a distributed load-balancing gateway architecture for data center networks. Based on this architecture, the overall design of the intelligent gateway was realized by field programmable gate array (FPGA). Jiang and Yang [20] proposed a finite-state intelligent monitoring method for distributed network anomaly attacks based on data fusion. Experimental results show that the proposed method can accurately determine the abnormal attack state and reduce the false positive rate and packet loss rate. Wu and Qi [21] proposed a false data recognition method based on the distributed spatial state model combined with extended Kalman and proved that the proposed new method has better detection rate and false alarm rate in the false and invalid data identification of distributed network users. Zhu [22] proposed a distributed data real-time encryption method for multilayer difference networks based on the elliptic curve encryption algorithm. The distributed data transmission is stable based on the elliptic curve encryption method, and the encryption of

distributed data takes a short time. Bao [23] proposed a fast acquisition method of resource user information based on the BP neural network, which supplements the missing scale of the original signal of the data structure. He and Pan [24] proposed a distributed localization algorithm based on second-order cone programming. Experimental data shows that the algorithm reduces the root mean square error and improves the positioning accuracy. Based on the distributed multitarget positioning system of the optical wavelength division multiplexing network, Zhu et al. [25] realized the 2-dimensional positioning of two targets with a maximum error of 7.09 cm and verified the reconfigurability of the system architecture.

In order to solve the problem of inconvenient operation and low accuracy of image processing and transmission system, this paper proposes a more accurate gradient calculation method based on the SIFT algorithm by studying the distributed network image processing system and transmission control algorithm, without losing image feature information. On the basis of quantity, the original algorithm and the improved algorithm performance of different sizes, different angles, and different scales are compared; the distributed storage and processing matching method of images is realized, and the image retrieval system in the single environment and distributed environment is compared. The influence of the image feature extraction rate is introduced. The distributed compression sensing technology is introduced in detail, and various measurement matrices are compared through experiments to reconstruct the performance of the algorithm. The algorithm BCS-SPL with better performance under distributed compressed sensing is introduced. As a result, it can be found that different orthogonal bases behave differently under different images.

2. Method

2.1. Image Feature Extraction

2.1.1. SIFT Algorithm. SIFT (scale-invariant feature transform) is a kind of image feature that satisfies the scale-invariant property. The SIFT algorithm has good stability to scale transformation, rotation transformation, and scaling transformation of images, and SIFT features have better uniqueness. It has strong discriminating ability; SURF algorithm (with acceleration robust features) uses integral graphs to accelerate the SIFT algorithm. The time of the SURF algorithm is about one-third of the SIFT algorithm. The dimension of the extracted feature vector is one dimension of the feature vector dimension extracted by the SIFT algorithm; the PCA-SIFT algorithm is also improved based on the scale-invariant feature transform algorithm. It is introduced into the principal component analysis method to extract the main information in the original feature vector, and the feature's vector is extracted to achieve the dimensionality reduction of the SIFT feature vector, which reduces the redundancy of the feature vector. Table 1 is a comparison table of the three image feature extraction algorithms.

It can be seen from the comparison of Table 1 that the three algorithms of SIFT, PCA-SIFT, and SURF have their own characteristic advantages. In terms of algorithm performance, PCA-SIFT is relatively moderate, always between SIFT and SURF. The SIFT algorithm has the best robustness in scale transformation and rotation transformation. The SURF algorithm is used for illumination. Changes and algorithms are most time-consuming. In the image retrieval system, the antiscale transformation, rotation transformation, and affine transformation of the image are relatively high, so the SIFT algorithm is very suitable as an image feature in the image retrieval system.

2.1.2. DCT Algorithm. Let the sequence $f(i)$ ($i = 0, 1, \dots, N - 1$) formed by the one-dimensional matrix be N , where N is the number of elements of the sequence, then the DCT of $f(i)$ is transformed into $F(u)$, and $F(u)$ satisfies the following formula:

$$F(u) = c(u) \sum_{i=0}^{N-1} f(i) \cos \left[\frac{(i+0.5)\pi}{N} u \right], \quad (1)$$

where $c(u)$ is its corresponding cosine coefficient and satisfies the following formula:

$$c(u) = \begin{cases} \sqrt{\frac{1}{N}}, & u = 0, \\ \sqrt{\frac{2}{N}}, & u \neq 0. \end{cases} \quad (2)$$

Let the two-dimensional discrete sequence formed by the two-dimensional matrix be $f(i, j)$ ($i = 0, 1, \dots, N - 1; j = 0, 1, \dots, N - 1$), where N is the length of the two-dimensional matrix, then the DCT of $f(i, j)$ is transformed into $f(u, v)$, which satisfies the following formula:

$$F(u, v) = c(u)c(v) \sum_{i=0}^{N-1} \sum_{j=0}^{N-1} f(i, j) \cos \left[\frac{(i+0.5)\pi}{N} u \right] \cdot \cos \left[\frac{(j+0.5)\pi}{N} v \right]. \quad (3)$$

The DCT transform is changed according to the DFT transform, both of which belong to the transform compression method, which can redistribute the information of the image. The DCT transform can make the image information mainly distributed in the upper left corner of the two-dimensional matrix, thereby facilitating the filtering of the image. At the same time, the two-dimensional matrix can be intercepted without losing the original information.

2.2. Image Feature Matching

2.2.1. Generate DoG Scale Space. The image of this series is the scale space $L(x, y, \sigma)$ of the original image, which is obtained by convolution of a variable-scale Gaussian function $G(x, y, \sigma)$ and image $I(x, y)$, namely,

TABLE 1: Comparison of SIFT, PCA-SIFT, and SURF characteristics under various transformations.

| Algorithm | Filter | Illumination | Scale | Affine transformation | Rotate | Time consumption |
|-----------|---------|--------------|---------|-----------------------|---------|------------------|
| SIFT | General | General | Good | Better | Good | General |
| PCA-SIFT | Good | Better | Better | Good | Better | Better |
| SURF | Better | Good | General | Better | General | Good |

$$L(x, y, \sigma) = G(x, y, \sigma) * I(x, y), \quad (4)$$

where $*$ indicates that the Gaussian function G performs a convolution operation in both the x and y directions, and the Gaussian function $G(x, y, \sigma)$ is

$$G(x, y, \sigma) = \frac{1}{2\pi\sigma^2} e^{-(x^2+y^2)/2\sigma^2}. \quad (5)$$

After obtaining the Gaussian pyramid of the image, the Gaussian difference image DoG (Difference of Gaussians) can be obtained by making Gaussian images of adjacent scales different. Record the response image of the Gaussian difference image $D(x, y, \sigma)$: k is the adjacent scale space multiple of the image.

2.2.2. Calculation of the Key Point Gradient. First, use $A, B, C,$ and D to solve the gradient of the pixel point O . $\text{grad } I_1(x, y)$ is recorded that the gradient of the pixel point O is solved by using $a, b, c,$ and d , in which $\text{grad } I_2(x, y)$ is recorded as follows:

$$\text{grad } I_1(x, y) = \left(\frac{\partial I_1}{\partial x}, \frac{\partial I_1}{\partial y} \right) = \left(\frac{y_D - y_s, y_c - y_A}{x_D - x_B, x_c - x_A} \right), \quad (6)$$

$$\text{grad } I_2(x, y) = \left(\frac{\partial I_2}{\partial x}, \frac{\partial I_2}{\partial y} \right) = \left(\frac{y_d - y_b, y_c - y_c}{x_d - x_b, x_c - x_a} \right),$$

where I_1 is the pixel function used to solve and I_2 is the pixel function used to solve the flip.

The gradient of pixel O is $\text{grad } I(x, y) = 1/2(\text{grad } I_1(x, y) + \text{grad } I_2(x, y))$.

The amplitude of pixel O is $m(x, y) = 1/2 \sqrt{\text{grad } I_1(x, y)^2 + \text{grad } I_2(x, y)^2}$.

The angle of pixel O is $\theta(x, y) = 1/2 (\theta_1(x, y) + \theta_2(x, y))$.

2.3. Image Transmission Technology

2.3.1. Block Compression Sensing. An image is divided into small blocks of $B \times B$ and then linearly measured using the same measurement matrix φ for each small block. Let x_j be the j th image subblock, and its corresponding measured value y_j can be expressed as

$$y_j = \Phi_B x_j, \quad (7)$$

where Φ_B is a matrix of $M_B \times B^2$ dimensions and x_j is a vectorized image block, and its sampling rate can be expressed as $R_s = M_B/B^2$. If the base matrix used is a two-dimensional DCT matrix, then the threshold function is as follows:

$$x = \begin{cases} x, & |x| \geq \tau, \\ 0, & \text{else,} \end{cases} \quad (8)$$

where $\tau = \lambda\sigma\sqrt{2 \log K}$, λ is a fixed parameter, and K is the number of transform coefficients. $\sigma = \text{median}(|x|)/0.6745$.

For DWT, this kind of transformation that needs to compare sparse parent-child transformations can be used:

$$\text{Threshold}(\xi, \lambda) = \frac{\left(\sqrt{\xi^2 + \xi_p^2} - \lambda(\sqrt{3}\sigma/\sigma_\xi) \right)_+}{\sqrt{\xi^2 + \xi_p^2}} \cdot \xi, \quad (9)$$

where ξ is the transform coefficient, ξ_p is its parent transform coefficient, λ is the constant, σ is the same as above, and σ_ξ is the edge test at 3×3 of the block size.

2.3.2. Intraprediction. Let the original signal be x and the predicted signal be \tilde{x} , then the residual can be expressed as

$$r = x - \tilde{x}. \quad (10)$$

In order to make the residual more sparse, that is, \tilde{x} to be closer to x , it can be described as the following form:

$$\begin{aligned} \tilde{x} &= \underset{p \in \mathbb{P}(x_{w_j})}{\text{argmin}} \\ &= \|x - p\|_2^2, \end{aligned} \quad (11)$$

where $P(x_{\text{ref}})$ represents a set of all prediction signals that can be obtained by the reference signal x_{ref} . Since the original signal x is unknown, other algorithms, such as the BCS-SPL algorithm, can be used instead of the calculated reconstructed signal:

$$\begin{aligned} \tilde{x} &= \underset{p \in \mathbb{P}(x_{w_j})}{\text{argmin}} \\ &= \|\hat{x} - p\|_2^2. \end{aligned} \quad (12)$$

The algorithm first uses the reconstructed signal calculated by BCS-SPL as the initialization signal, then predicts the original signal based on the measured value, and then adds the residual signal to the reconstructed signal. The above prediction and reconstruction are performed again by comparing the SSM value and the residual difference adjustment parameters. Through repeated iterations, the final reconstruction effect is improved. At present, base matrices such as DFT, DCT, DWT, and DDWT (dual-tree DWT) and contourlet transform CT (contourlet transform) can be used. Some people have proposed the MS-BCS-SPL (multiscale BCS-SPL) algorithm, which uses the layering characteristics of wavelet transform coefficients to use different sampling rates for different layers.

2.4. Transmission Channel

2.4.1. Softcast. In order to remove the redundancy of the image, Softcast performs DCT transform on the MPEG-like image, then divides the DCT transform coefficients into small blocks, and discards the block with the coefficient of 0. Compression is achieved by transmitting only nonzero coefficient blocks and their location. In a limited bandwidth, if a nonzero coefficient block needs to be discarded, the coefficient block with low energy is preferentially discarded because these coefficients contribute less to reconstruction during reconstruction. In order to reduce the influence of noise during transmission, the transmission power of the transmitting end can be increased under the condition that the noise power is constant. However, in the case where the total power at the transmitting end is constant, in order to minimize the reconstruction error, each block of power can be reallocated, and the power is allocated as follows:

$$\mu_i[j] = g_i x_i[j], \quad (13)$$

where $g_i = \lambda_i^{-1/4} (\sqrt{p/\sum_i \sqrt{\lambda_i}})$ is the energy weighting factor, P represents the total energy, and λ_i represents the variance of the DCT coefficients of the i th block.

2.4.2. Image Transmission Framework Based on Block Compression Sensing. In this paper, only additive white Gaussian noise (AWGN) is considered, and its noise energy is E_0 ; its channel signal-to-noise ratio (CSNR) can be expressed by the following formula:

$$\text{CSNR} = \frac{\|y\|_2^2}{\|e\|_2^2}. \quad (14)$$

In order to facilitate the subsequent experimental comparison, for the coding system, the image is first divided into blocks, and then, a measurement matrix $\Phi \in \mathbb{R}^{N \times N}$ is used for measurement, that is, the sampling rate is 1. The resulting measurements are interleaved because the measurement of an entire block is not lost when the packet is lost. The effect of packet loss is not concentrated in a certain area, but distributed over the entire image. Avoid situations where a blocky irrational area that throws a packet causes visibility of the entire image.

3. Experiment

3.1. Experimental Platform. This system requires 5 machine nodes, but the computer resources are limited. This system only uses 2 computers. Install VMware Workstation software on these 2 computers to build 5 virtual machines. Each virtual machine is installed with CentOS6.5. The operating system and the five virtual machines are connected to the same router so that they are on the same LAN so that they can access each other. The software and hardware of each virtual machine are shown in following Tables 2 and 3 .

3.2. Test Dataset. The dataset used in this system is provided by a large-scale image data research team from France. The team has collected a large number of images taken in various

TABLE 2: System operating environment.

| Virtual machine version | VMware Workstation 10.0.1 |
|-------------------------|---------------------------|
| Operating system | Centos6.5 |
| Hadoop version | hadoop2.7 |
| JDK version | jdk.7 |
| Number of nodes | 5 |

TABLE 3: Basic hardware of each host.

| Hostname | Number of processors | Memory size | Hard disk size |
|------------------|----------------------|-------------|----------------|
| hadoop01.seu.com | 4 | 4 | 60 |
| hadoop02.seu.com | 4 | 6 | 60 |
| hadoop03.seu.com | 2 | 1.5 | 60 |

scenes since 2003. The dataset used in this system contains hundreds of different types. The image of the category has a total of 3,401 images and a size of 1.02 GB. These images are in various formats and satisfy the image application scenarios required by the image search system.

The system uses these image data as the image library of the image retrieval system. For the convenience of management, the system stores the image data to be used in 12 different folders, and the image size and the number of images in each folder are not similar, and the folder size and number of images for each folder are shown in Table 4.

After the image datasets are obtained, these datasets are only stored on the disk of the local file system of a single computer. To distribute the image data, the image dataset needs to be transferred to the HDFS. The main purpose of this section is to generate the hib and dat files of the image set and store them on HDFS. You need to download and install the HIPI tool before generating hib and other files. The distributed use of HIPI requires the use of the Gradle automated build system, which is used to manage compilation and package installation of HIPI. The best way to get the latest version of HBPI is by cloning the official GitHub repository and building all of its tools and sample programs.

4. Results

4.1. Image Feature Extraction Analysis. The extracted feature points of the original image are shown in Figure 1. The figure contains feature point information at different scales, and these feature points are marked on the original image. Each key point in the figure consists of a circle and a line segment. The circle represents different scales. The larger the circle, the larger the scale represented by the circle. The direction indicated by the line segment on the circle represents the direction of the feature point. It can be seen from the figure that the image feature points always appear where the pixel values jump, and the more the pixels in the local region jump, the more the feature points in the region.

The above simulation process proves that the image feature extraction algorithm proposed in this paper is feasible. Compared with the time spent running the feature extraction algorithm on the local and the time taken to extract the image features distributed under the cluster, the

TABLE 4: Image dataset.

| Dataset | Number of images | Dataset size |
|-----------|------------------|--------------|
| All-souls | 132 | 49.4 |
| Ashmolean | 195 | 72.4 |
| Balliol | 154 | 61.4 |
| Bole | 214 | 79.5 |
| Chri | 543 | 227 |
| Corn | 59 | 20.3 |
| Hertford | 67 | 26.1 |
| Jesus | 161 | 65.6 |
| Keble | 121 | 44.0 |
| Marry | 689 | 232.0 |
| New | 105 | 41.7 |
| Pictures | 149 | 56.3 |



FIGURE 1: Image feature extraction.

impact on the performance of the image feature extraction algorithm when the number of nodes is different in the cluster is also studied. Table 5 shows the running time of the image feature extraction algorithm under different conditions.

Figure 2 shows the time it takes to run image feature extraction locally and the time spent in the cluster environment as the number of nodes increases.

It can be seen from the figure that when the number of nodes in the cluster is larger, the image feature extraction of the same group of images takes less time and tends to be flat. In fact, the local running feature extraction algorithm and the node have only one distributed operation, and both have only one running node, but the distributed extraction of one node takes slightly more time than the local one, because distributed operation is used not only to perform a feature extraction task but also to execute other programs. When the number of nodes increases, it will run more efficiently than local ones, and it can be greatly improved in performance.

4.2. Image Feature Matching Analysis. Different sizes of images will affect the matching effect of the image. Figure 3 shows the matching result between the image after the expansion and transformation, and the original image is doubled. The feature extraction algorithm is extracted by the

TABLE 5: Run time of the image feature extraction algorithm under different conditions.

| Number of nodes | Local operation | 1 | 2 | 3 | 4 | 5 |
|-------------------------|-----------------|-----|----|----|----|----|
| Feature extraction time | 413 | 447 | 92 | 66 | 58 | 54 |

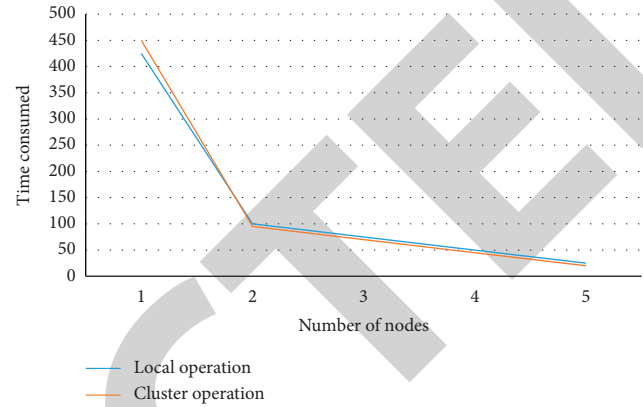


FIGURE 2: The running time of the image feature extraction algorithm under different conditions.

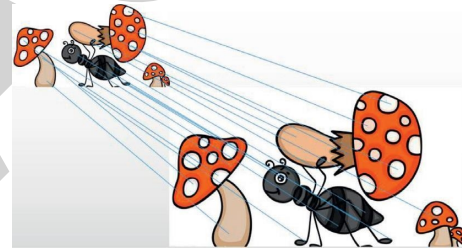


FIGURE 3: Scaling transformation matching graph.

feature extraction algorithm proposed in this paper. Then, matching with the original image, the two endpoints of each line segment in the figure represent the matching points in the two images. It can be seen from the figure that, after the image is scaled, the image features extracted by the system are not changing too much; the image-matching point between the two images is basically correct.

Figure 3 shows the case where the expansion factor is 2. However, as the image expansion coefficient changes, the matching effect of the image changes. Different feature descriptors have different matching effects on the image. Figure 4 shows the original image undergoing different scaling. The performance comparison chart of the image matching operation between the transformed image and the original image is shown in Figure 4. The improved SIFT algorithm is an improved algorithm based on SIFT proposed by the system. It can be seen that the improved SIFT algorithm has more matching points than the original algorithm; when the expansion coefficient of the image is closer to 1, the more the matching points of the image, the smaller the number of matching points of the image as the stretching coefficient is away from 1, but there are still many matching points between the image after scaling and the original image, so reducing the matching points will not affect the matching result between the two images.

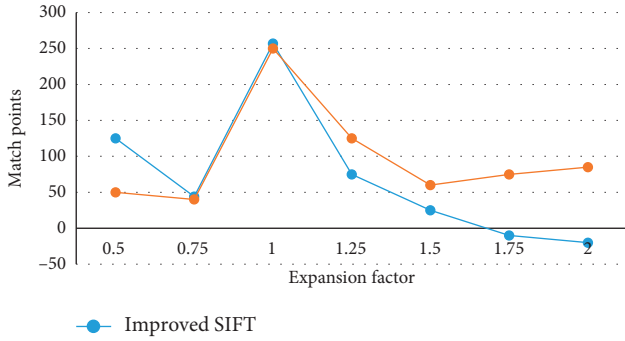


FIGURE 4: Matching results at different sizes.

The scale transformation is also an important factor affecting the image-matching effect. Figure 5 shows the matching result of the image after the scale transformation and the original image. The image on the right side of the image is the image after the original image has been Gaussian blurred, which is different from the original image. On the scale, it can be seen that the scale transformation does not change the image features of the original image too much. Most of the matching pairs are successfully matched, and a small number of mismatched points appear, but it is also within the acceptable range. Figure 6 shows the result of image-matching operation between the original image and the original image after different Gaussian function blurring.

The improved SIFT algorithm in the figure is the improved SIFT algorithm of the system. It can be seen from the figure that the matching points of the improved algorithm of the system are slightly higher than the original algorithm. The Gaussian window used here is a 5×5 matrix, the abscissa represents the variance of the Gaussian matrix, and the ordinate represents the number of matching points of the two images at different scales. It can be seen from the figure that, as the image scale becomes larger between the two images, the number of matching points is gradually decreasing, and it can also be shown that the image features extracted by the system can still find corresponding matching points in images of different scales.

4.3. Image Transmission Path Analysis. Figure 7 compares the reconstruction performance of the BCS-SPL algorithm under different orthogonal basis. In order to compare the experimental results, the experiment uses the original OMP algorithm for comparison. The OMP algorithm processes the sparse representation of the original signal to obtain a good reconstruction effect. The experimental image is a 512×512 lena image with a block size of 32, where DWT uses the 9-7DWT algorithm; BCS-SPL-DFT has a λ value of 0.35; The λ values of BCS-SPL-DCT 6, BCS-SPL-CT and BCS SPL-DDWT, BCS-SPL-DWT are 10, 25 and 25, 20, respectively. It can be seen from Figure 7 that the BCS-SPL's algorithm has a good reconstruction effect, and it can still achieve a reconstructed PSNR of 28 dB in the case of a sampling rate of 0.1. Comparing the BCS-SPL algorithm using different orthogonal bases, it can be seen that BCS-SPL-DDWT works best, followed by BCS-SPL-CT and

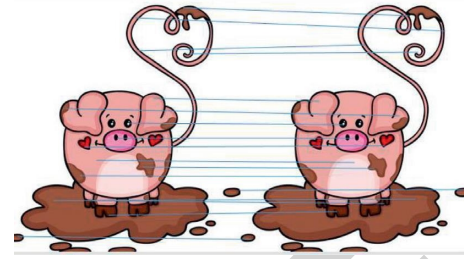


FIGURE 5: Scale transformation matching graph.

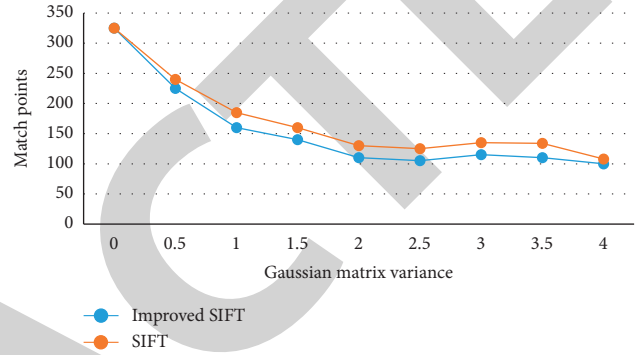


FIGURE 6: Matching results at different scales.

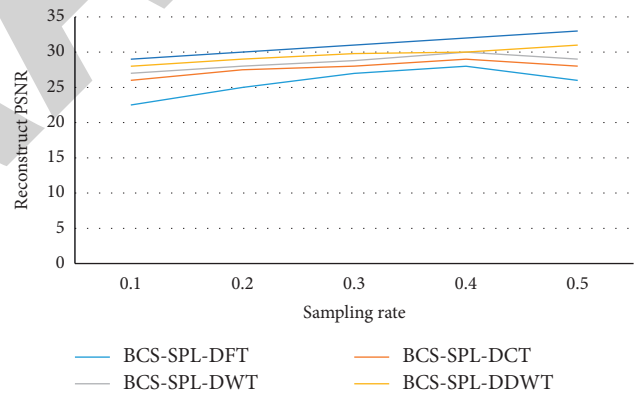


FIGURE 7: Comparison of BCS-SPL algorithm and OMP algorithm reconstruction under different orthogonal basis.

BCS-SPL-DWT. The reason for this situation is that the orthogonal basis of the image is more sparse; the smaller the K value, the better the final reconstruction effect after enough iterations. Therefore, in order to obtain a better reconstruction effect, an orthogonal basis or a dictionary that makes the image more sparse can be used.

Table 6 shows the time taken for the various algorithms to reconstruct the original image at various sampling rates during the experiment in Figure 7. It can be seen from the table that the BCS-SPL algorithm is a very fast algorithm. It is 10 times faster than the OMP algorithm at a sampling rate of 0.5 and is essentially flat at low sampling rates. Moreover, it can be seen from the comparison that the algorithm time consumption of BCS-SPL decreases with the increase of the sampling rate, and the OMP algorithm is just the opposite. This is because BCS-SPL first calculates a rough result and

TABLE 6: Time taken in the experiment above.

| | 0.1 | 0.2 | 0.3 | 0.4 | 0.5 |
|--------------|-------|-------|-------|-------|--------|
| BCS-SPL-DFT | 11.69 | 11.43 | 13.15 | 10.14 | 7.64 |
| BCS-SPL-DCT | 11.35 | 6.76 | 6.84 | 5.32 | 5.62 |
| BCS-SPL-DWT | 18.88 | 10.60 | 6.05 | 3.81 | 4.35 |
| BCS-SPL-DDWT | 27.74 | 13.54 | 9.1 | 5.31 | 6.21 |
| BCS-SPL-CT | 18.47 | 8.16 | 6.31 | 4.25 | 4.35 |
| OMP | 14.65 | 30.52 | 50.12 | 75.34 | 115.94 |

then iteratively makes the result step by step better, so in the case of more information, it can get good results from the beginning. It is often not necessary to complete the entire iterative process to reach the bounce condition, which can effectively save computing time. The higher the sample rate of the OMP algorithm, the more optimal the current signal needs to be selected, so the time consumption increases as the sampling rate increases.

4.4. Image Transmission Control Analysis. Figure 8 compares the reconstructed images of the several algorithms above with a Y component sampling rate of 0.2 and a cbr component of 0.05. It can be seen from the figure that the effects of several algorithms are not bad. The image of BCS-SPL-DDWT is slightly blurred, and MH+BCS-SPL and BCS-SPL-DDWT have some color distortions in the four corners. The MH-BCS-SPL algorithm performs best. In order to visually compare the actual effects of the two transmission frames, the experiment used a lena image as the transmission image. Compared with the noiseless and CSNR 20db channel and the packet loss rate of 0.1–0.6, the reconstruction effect of the image transmission framework and Softcast framework based on the block compression perception is compared. In order to remove the influence of the orthogonal basis matrix, the reconstruction algorithm of the image frame based on block compression sensing uses BCS-SPL-DCT and MH-BCS-SPL, and the initial predicted image of MH-BCS-SPL and BCS-SPL-DCT is generated. The block size in the experiment was 32×32 . The experimental results are shown in Figure 9.

It can be seen from the figure that the image transmission framework based on the distributed network has a significant improvement compared with Softcast in the absence of noise but packet loss. The MH-BCS-SPL reconstruction algorithm works best, and the PSNR decreases very smoothly in the process of increasing the packet loss rate from 0.1 to 0.6. The BCS-SPL-DCT algorithm works well, and the reconstruction time is very low, but the fluctuation is slightly larger; Softcast's refactoring effect is obviously not as good as the above algorithm, and the downward trend is even greater.

5. Discussions

The simulation realizes the matching of images under different conditions and analyzes the matching ability of image matching with different scales, different angles, and different sizes. Figures 1 and 2 strongly prove the image features and corresponding extraction by the system. The effectiveness of

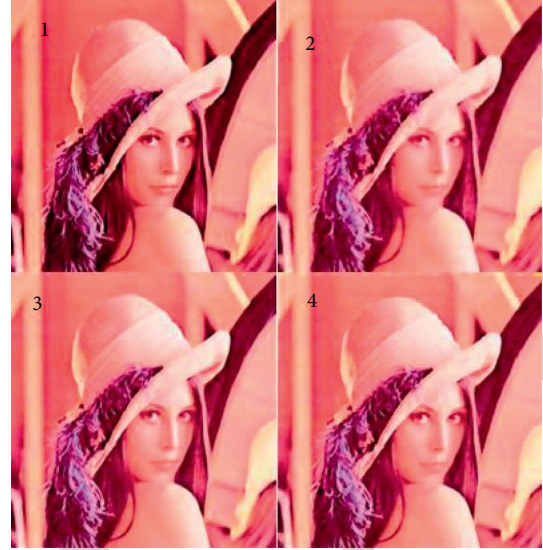


FIGURE 8: Comparison of several reconstruction algorithms.

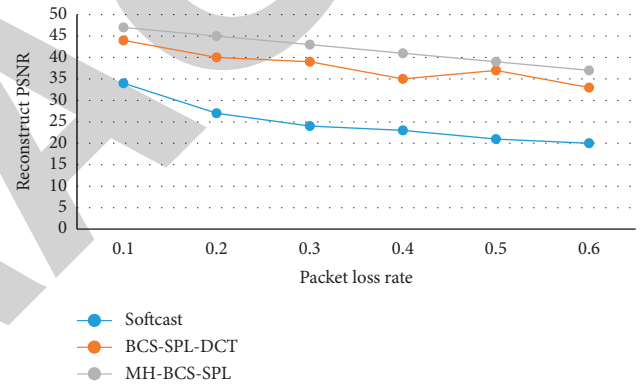


FIGURE 9: Comparison of reconstruction effects of various image transmission frameworks.

the image feature matching method is also compared with the image feature extraction algorithm and the image feature extracted by the SIFT algorithm. The image feature extraction algorithm and corresponding image are presented.

On the basis of ensuring the good local features of SIFT, the SIFT is improved by combining the spatial relationship features of local images and DCT transform so that the image features are more accurately described, and the dimension of the final descriptor is 65 dimensions. Finally, the image feature extraction is simulated and analyzed. The feasibility of the feature extraction algorithm proposed in this paper and the efficiency of the distributed feature extraction algorithm are proved from Figures 3–6.

The improvement of the BCS-SPL algorithm by the MH-BCS-SPL algorithm is compared by Figure 7. As far as the static image is concerned, the reconstruction performance of the algorithm is further improved by increasing the prediction. The experiment proves that the image transmission framework based on the distributed network has a good reconstruction effect, and it still has a good performance under the condition of high packet loss rate. However, due to

the limited noise immunity of the reconstruction algorithm itself, it is generally performed in the case of low signal-to-noise ratio.

It can be seen from Figures 8 and 9 that the performance of the MH-BCS-SPL algorithm is the best, and these algorithms can achieve good results. The above experiment proves that, for color images, it is very effective to use a lower sampling rate for the chrominance components. In addition to the above algorithms, there are other algorithms for processing color images using compressed sensing, but these algorithms have no obvious effect, and the computational complexity is not reduced.

6. Conclusion

By studying the distributed network image processing system and transmission control algorithm, this paper draws the following conclusions:

- (1) This paper proposes a more accurate gradient calculation method based on the SIFT algorithm. Based on the loss of image feature information, the performance of the original algorithm and the improved algorithm of different sizes, angles, and scales are compared. The performance of the proposed algorithm is slightly better than that of the original algorithm. Therefore, the system can effectively reduce the dimension of image features without reducing the performance of the original algorithm.
- (2) This paper implements a distributed storage and processing matching method for images. By comparing the effects of the image retrieval system in the single-machine environment and distributed environment on the image feature extraction rate, it is proved that the image feature extraction rate in the distributed environment is 5–8 times faster than that in the stand-alone environment. When the number of machine nodes increases, the efficiency of distributed feature extraction will be higher and higher, but in the end, it will be flat. The image retrieval system built by the system with 5 distributed nodes achieves the best results in terms of machine cost and system performance.
- (3) The distributed compressed sensing technology is introduced in detail, and various measurement matrices are compared through experiments to reconstruct the performance of the algorithm. The random Gaussian orthogonal matrix is analyzed with good stability and performance. The OMP algorithm has good convergence and reconstruction performance.
- (4) Introduced the BCS-SPL algorithm with better performance under distributed compressed sensing. The experimental results show that different orthogonal bases behave differently under different images. Overall, the BCS-SPL series algorithm has greatly improved the reconstruction effect compared with the traditional OMP algorithm. In addition, the

time consumption of different algorithms is compared experimentally. Unlike the OMP algorithm, the BCS-SPL algorithm takes more time in the case of low sampling rate. These algorithms are used to analyze the image transmission framework based on distributed compressed sensing, which is applied in the wireless multiuser transmission environment and compared with Softcast through experiments.

Data Availability

No data were used to support this study.

Conflicts of Interest

The authors declare that they have no conflicts of interest.

Acknowledgments

This work was supported by Excellent Talents Foundation of China West Normal University (nos. 17YC497 and 17YC498).

References

- [1] W. Kim, "A design and implementation of the real time 4-channel image processing system for vehicle using the smart phone," *Advanced Science Letters*, vol. 23, no. 4, pp. 3763–3766, 2017.
- [2] C. H. G. Wright, S. F. Barrett, D. J. Pack, T. R. Schei, J. R. Anderson, and M. J. Wilcox, "Computational image processing for a computer vision system using biomimetic sensors and eigenspace object models," in *Proceedings of SPIE-The International Society for Optical Engineering*, vol. 5299, pp. 327–336, 2017.
- [3] B. Mataei, F. Moghadas Nejad, M. Zahedi, and H. Zakeri, "Evaluation of pavement surface drainage using an automated image acquisition and processing system," *Automation in Construction*, vol. 86, pp. 240–255, 2018.
- [4] F. R. Barceló, P. J. D. Hierro, F. R. Llario et al., "Development of an ultrasonic weld inspection system based on image processing and neural networks," *Nondestructive Testing & Evaluation*, vol. 33, no. 1, pp. 1–8, 2018.
- [5] Á. Borsos, B. Szilágyi, P. Ş. Agachi, and Z. K. Nagy, "Real-time image processing based online feedback control system for cooling batch crystallization," *Organic Process Research & Development*, vol. 21, no. 4, pp. 511–519, 2017.
- [6] Mu Xiao, "Application of UAV and image processing technology in oil and gas field production," *Digital Communication World*, vol. 02, p. 196+269, 2019.
- [7] W. Qiao and X. Tian, "Design of video image data processing system in airborne live video recording and transmission system," *Ship Electronic Engineering*, vol. 38, no. 11, pp. 102–105, 2018.
- [8] X. Zhang, "Analysis of computer image processing technology," *Electronic Technology and Software Engineering*, vol. 19, p. 136, 2018.
- [9] X. Zhang, X. Sun, and L. Zhang, "Design of online insulator image acquisition and real-time processing system," *Electronic Measurement Technology*, vol. 41, no. 16, pp. 113–118, 2018.
- [10] X. Zhang, J. Wang, K. Peng et al., "Rice grain counting system based on image processing and Bluetooth transmission

- technology,” *Shandong Agricultural Sciences*, vol. 50, no. 07, pp. 157–160, 2018.
- [11] L. Cong, C. Huang, and C. An, “Design of real-time infrared image processing simulation platform based on DSP6455,” *Laser & Infrared*, vol. 48, no. 06, pp. 726–729, 2018.
- [12] B. Li, X. Liu, W. Yang, and C. Liu, “A design of high speed image data transmission based on RapidIO bus,” *Space Control*, vol. 36, no. 01, pp. 69–74, 2018.
- [13] W. Zhang, R. Fan, R. Gong, and Y. Huan, “Wireless remote fire extinguishing of intelligent car based on image processing,” *Laboratory Research and Exploration*, vol. 37, no. 01, pp. 33–37, 2018.
- [14] E. I. Benchimol, C. N. Bernstein, A. Bitton et al., “Trends in epidemiology of pediatric inflammatory bowel disease in Canada: distributed network analysis of multiple population-based provincial health administrative databases,” *American Journal of Gastroenterology*, vol. 112, no. 7, pp. 1120–1134, 2017.
- [15] L. Rupprecht, W. Culhane, and P. Pietzuch, “SquirrelJoin,” *Proceedings of the VLDB Endowment*, vol. 10, no. 11, pp. 1250–1261, 2017.
- [16] A. Awad, A. Mohamed, C.-F. Chiasserini, and T. Elfouly, “Distributed in-network processing and resource optimization over mobile-health systems,” *Journal of Network and Computer Applications*, vol. 82, pp. 65–76, 2017.
- [17] R. Zhou and Q. Liang, “Distributed digital rights management mechanism based on blockchain credit system,” *Computer Application Research*, vol. 2019, 6 pages, 2019.
- [18] W. Li, “Research on active intrusion prevention technology of distributed automation network,” *Automation & Instrumentation*, vol. 04, pp. 159–162, 2019.
- [19] Y. Lan, Z. Sun, and L. Dong, “Distributed load balancing gateway architecture for data center networks,” *Journal of Terahertz Science and Electronics Information*, vol. 17, no. 02, pp. 315–321, 2019.
- [20] G. Jiang and L. Yang, “A finite state intelligent monitoring simulation for distributed network anomaly attacks,” *Computer Simulation*, vol. 04, pp. 256–259+264, 2019.
- [21] Z. Wu and J. Qi, “Actuation of accurate identification of false data in distributed network information,” *Computer Simulation*, vol. 04, pp. 269–272, 2019.
- [22] X. Zhu, “Remote data real-time encryption simulation of multi-layer difference network,” *Computer Simulation*, vol. 04, pp. 273–276+314, 2019.
- [23] Z. Bao, “Rapid acquisition of distributed network resource user information simulation,” *Computer Simulation*, vol. 04, pp. 345–348, 2019.
- [24] W. He and L. Pan, “Research on distributed cooperative location of mobile wireless sensor networks,” *Computer Applications and Software*, vol. 36, no. 04, pp. 161–165, 2019.
- [25] D. Zhu, W. Xu, W. Chen, L. Jiang, and S. Pan, “Distributed multi-target positioning system based on optical wavelength division multiplexing network,” *Journal of Radar*, vol. 8, no. 02, pp. 171–177, 2019.